Distributions of particulate Heme *b* in the Atlantic and Southern Oceans—Implications for electron transport in phytoplankton

Martha Gledhill,[1,2] Eric P. Achterberg,[1,2] David J. Honey,[1] Maria C. Nielsdottir,[1,3] and Micha J. A. Rijkenberg [1,4]

Received 22 April 2013; revised 19 September 2013; accepted 17 October 2013; published 12 November 2013.

[1] Concentrations of heme *b*, the iron-containing component of *b*-type hemoproteins, ranged from < 0.4 to 5.3 pM with an average of 1.18 ± 0.8 pM (± 1σ; $n = 86$) in the Iceland Basin (IB), from < 0.4 to 19.1 pM with an average of 2.24 ± 1.67 pM ($n = 269$) in the tropical northeast Atlantic (TNA) and from 0.6 to 21 pM with an average of 5.1 ± 4.8 pM ($n = 34$) in the Scotia Sea (SS). Heme *b* concentrations were enhanced in the photic zone and decreased with depth. Heme *b* concentrations correlated positively with chlorophyll *a* (chl *a*) in the TNA ($r = 0.41$, $p < 0.01$, $n = 269$). Heme *b* did not correlate with chl *a* in the IB or SS. In the IB and SS, stations with high-chlorophyll and low-nutrient (Fe and/or Si) concentrations exhibited low heme *b* concentrations relative to particulate organic carbon (< 0.1 μmol mol^{-1}), and high chl *a*:heme *b* ratios (> 500). High chl *a*:heme *b* ratios resulted from relative decreases in heme *b*, suggesting proteins such as cytochrome b_6f, the core complex of photosystem II, and eukaryotic nitrate reductase were depleted relative to proteins containing chlorophyll such as the eukaryotic light-harvesting antenna. Relative variations in heme *b*, particulate organic carbon, and chl *a* can thus be indicative of a physiological response of the phytoplankton community to the prevailing growth conditions, within the context of large-scale changes in phytoplankton community composition.

Citation: Gledhill, M., E. P. Achterberg, D. J. Honey, M. C. Nielsdottir, and M. J. A. Rijkenberg (2013), Distributions of particulate Heme *b* in the Atlantic and Southern Oceans—Implications for electron transport in phytoplankton, *Global Biogeochem. Cycles*, *27*, 1072–1082, doi:10.1002/2013GB004639.

1. Introduction

1.1. Heme *b*

[2] Oceanic phytoplankton are known to change the abundance of iron-containing proteins when nutrient concentrations or incident light levels change [*Pankowski and McMinn*, 2009; *Peers and Price*, 2006; *Saito et al*., 2011; *Strzepek and Harrison*, 2004; *Wolfe-Simon et al*., 2006]. The cellular abundance of such proteins influences the efficiency of photosynthesis [*Bailey et al*., 2008; *Cardol et al*., 2008; *Peers and Price*, 2006] and so links nutrient abundance and light to ocean productivity. Ferredoxin [*Mckay et al*., 1999; *Pankowski and McMinn*, 2009], photosystem I (PSI), cytochrome b_6f (cytb_6f) [*Eberhard et al*., 2008; *Saito et al*., 2011; *Strzepek and Harrison*, 2004], cytochrome c_{550} [*Saito et al*., 2011], soluble cytochrome c [*Eberhard et al*., 2008; *Peers and Price*, 2006], and iron superoxide dismutase [*Wolfe-Simon et al*., 2006] have all been shown to be reduced in abundance or replaced by noniron-containing proteins when oceanic phytoplankton are grown under low-iron or -nutrient conditions in the laboratory. Furthermore, recent work has shown downregulation of genes associated with iron proteins or iron protein synthesis [*Allen et al*., 2008; *Lommer et al*., 2012; *Thompson et al*., 2011] and diurnal cycling of iron protein pools in order to conserve iron use [*Saito et al*., 2011]. However, few studies have investigated the abundance of iron-containing proteins in the field or how their distributions are influenced by the prevailing nutrient and light regimes [*Erdner and Anderson*, 1999; *Pankowski and McMinn*, 2009]. Heme *b* is an iron-containing porphyrin which functions as a prosthetic group for proteins involved in electron transfer and the scavenging of reactive oxygen species [*Chapman et al*., 1997]. Heme *b* is highly toxic to cells if not incorporated into proteins [*Espinas et al*., 2012] and the stoichiometry of heme *b* within proteins is fixed [*Shekhawat and Verma*, 2010; *Tanaka and Tanaka*, 2007], so that changes in heme *b* abundance will reflect changes in the cellular abundance of heme *b*-containing proteins. In marine phytoplankton, heme *b* is incorporated into proteins involved in photosynthesis,

[1]School of Ocean and Earth Science, National Oceanography Centre, University of Southampton, Southampton, UK.
[2]Chemical Oceanography, Helmholtz Centre for Ocean Research (GEOMAR), Kiel, Germany.
[3]Department of Ocean, Earth, and Atmospheric Sciences, Old Dominion University, Norfolk, Virginia, USA.
[4]Royal Netherlands Institute for Sea Research, Den Burg, Netherlands.

Corresponding author: M. Gledhill, Chemical Oceanography, Helmholtz Centre for Ocean Research (GEOMAR), DE-24148 Kiel, Germany. (mgledhill@geomar.de)

© 2013 The Authors. *Global Biogeochemical Cycles* published by Wiley on behalf of the American Geophysical Union.
This is an open access article under the terms of the Creative Commons Attribution License, which permits use, distribution and reproduction in any medium, provided the original work is properly cited.
0886-6236/13/10.1002/2013GB004639

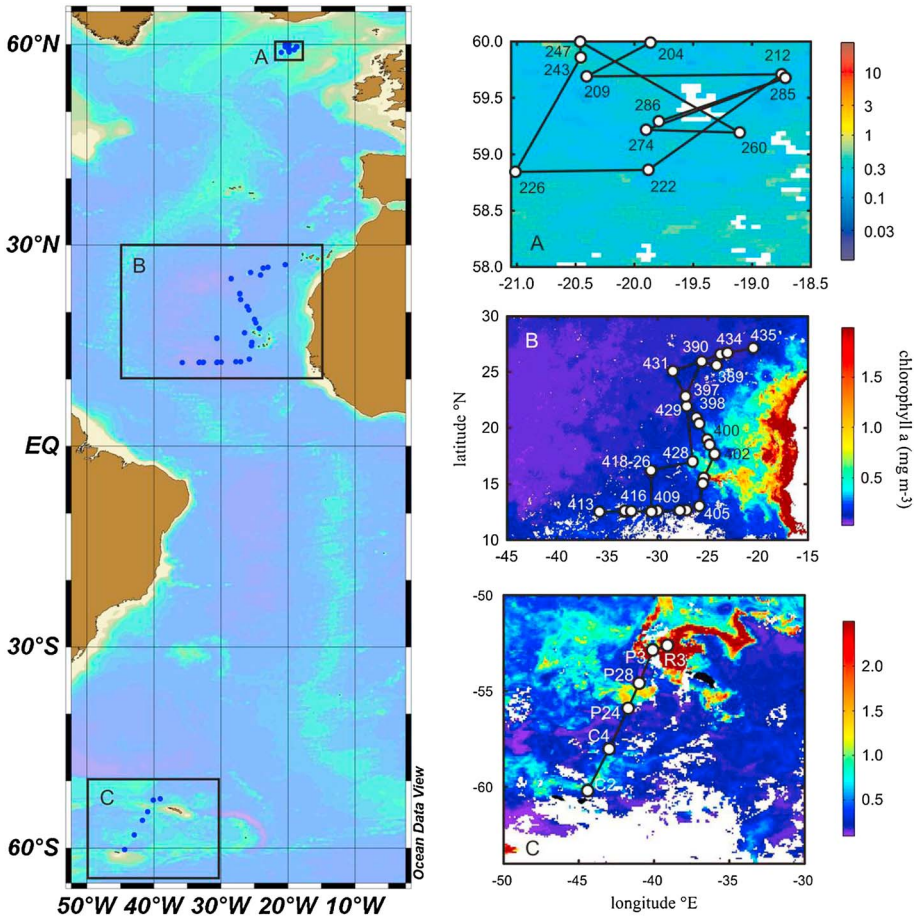

Figure 1. Map of the Atlantic Ocean showing the areas sampled. Inset maps show the sampled stations superimposed on average Sea-viewing Wide Field-of-view Sensor-derived chl *a* (mg m^{-3}) for the times of the cruises. (a) Iceland Basin, (b) tropical northeast Atlantic, and (c) Scotia Sea. Note that scale changes for chl *a*. Some station numbers are omitted in Figure 1b for clarity.

respiration, and reactive oxygen scavenging [*Honey et al.*, 2013]. Laboratory studies of marine eukaryotic phytoplankton showed that heme *b* concentrations extracted by ammoniacal detergent averaged 3.7 ± 0.9 μmol mol^{-1} C in resource replete conditions and that the cellular concentrations of heme *b* decreased under nutrient deplete conditions. Heme *b* accounted for $18 \pm 14\%$ of the total particulate iron pool when iron concentrations in the culture media were low. Decreases in heme *b* relative to particulate organic carbon (POC) were also observed to correspond with decreasing nitrate and phosphate concentrations across a transect of the (sub-) tropical North Atlantic. Chlorophyll *a*:heme *b* ratios were also found to vary for certain species when phytoplankton were grown under decreased iron, nitrate, or light conditions. However, results from the temperate and (sub-) tropical North Atlantic showed that chl *a*:heme *b* increased with depth and were thus driven by gradients in light rather than nutrients [*Honey et al.*, 2013]. Determination of the concentration of heme *b* in particulate material and comparison with phytoplankton biomass, POC, and chl *a* in the ocean could thus provide information on the variation in heme *b* protein abundance and the response of phytoplankton to prevailing nutrient and light conditions.

[3] In this study, we determined heme *b* in particulate material in three contrasting regions of the Atlantic Ocean and Southern Ocean: the Iceland Basin (IB), the tropical northeast Atlantic (TNA), and the Scotia Sea (SS). The IB is situated in the high-latitude North Atlantic and is characterized by pronounced diatom-dominated spring blooms [*Leblanc et al.*, 2009], which nevertheless do not result in the complete drawdown of nitrate and phosphate. Residual nutrient stocks are thus subsequently exploited by more mixed phytoplankton assemblages [*Leblanc et al.*, 2009; *Poulton et al.*, 2010]. The post spring bloom period is iron limited [*Nielsdottir et al.*, 2009], a result of both low atmospheric iron inputs [*Jickells et al.*, 2005] and suboptimal iron:nitrate ratios in winter-overturned deep waters [*Nielsdottir et al.*, 2009].

[4] The region of the TNA examined in this study is influenced in the east by the highly productive upwelling system off the Northwest African Coast, in the south by the oxygen minimum zone off the Cape Verde Islands and in the northwest by the permanently stratified oligotrophic subtropical North Atlantic Gyre [*Stramma et al.*, 2008]. Atmospheric iron inputs in this region are relatively high due to the influx of Saharan and Sahel dust [*Jickells et al.*, 2005; *Mulitza et al.*, 2010; *Stuut et al.*, 2005] with maximum dust inputs in this region occurring in winter (January to March) [*Chiapello et al.*, 1995]. The phytoplankton community in the TNA is dominated by picoplankton comprising *Prochlorococcus* sp., *Synechococcus* sp., and picoeukaryotes

Table 1. Heme *b* Extraction Efficiencies From Representative Hemoproteins Using Ammoniacal Detergent[a]

Hemoprotein	Recovery (%)	Approximate Distance Between Iron Atom and Protein Surface (Å)[d]	5th/6th Iron Ligand[b]	Spin State[b]
Catalase	8 ± 1[c]	>20	Tyrosine/H_2O	HS
Horseradish peroxidase	36 ± 4[c]	10–20	Histidine/H_2O	HS
Hemoglobin	76 ± 4	<10	Histidine/H_2O	HS/LS
Myoglobin	79 ± 2	<10	Histidine/H_2O	HS/LS
Cytochrome b_5	76 ± 1	<10	Histidine/Histidine	LS

[a]An estimate of exposure of the heme group to the solvent, expressed as the distance between the center of the heme group and the protein surface, the ligands occupying the fifth and sixth coordinate sites in the octahedrally complexed iron, and the spin state of iron in the complex are also provided.
[b]*Frausto da Silva and Williams*, 2001.
[c]*Honey et al*., 2013.
[d]Estimated using Chem3D Pro© from Protein Data Bank files for Bovine catalase (3NWL) [*Foroughi et al*., 2011], horseradish peroxidase (1HCH) [*Berglund et al*., 2002], hemoglobin (1GZX) [*Paoli et al*., 1996], myoglobin (2V1K) [*Hersleth et al*., 2007], and rat cytochrome b5 (1MNY) [*Banci et al*., 2001].

[*Hill et al*., 2010], although nitrogen-fixing *Trichodesmium* spp. are also observed in this region [*Moore et al*., 2009], with their abundance being tightly linked to dust inputs [*Rijkenberg et al*., 2011, 2012].

[5] The SS lies within the Atlantic sector of the Southern Ocean. The SS contrasts with much of the high-nutrient low-chlorophyll (HNLC) regions of the Southern Ocean as it supports extensive phytoplankton blooms, with the South Orkney Islands, the South Sandwich Islands, and South Georgia acting as potential sources of iron via the "island mass effect" [*Doty and Oguri*, 1956; *Korb et al*., 2005; *Nielsdottir et al*., 2012]. The waters around South Georgia are particularly productive and can support Antarctic diatom-dominated blooms of up to 12 mg m^{-3} chl *a* for periods of up to 5 months [*Korb et al*., 2005]. However, productivity in the area is patchy, and regions to the south of South Georgia have HNLC characteristics [*Hinz et al*., 2012; *Korb et al*., 2010].

[6] We compare the distribution of heme *b* to chl *a*, phytoplankton biomass, POC, and particulate organic nitrogen (PON) and interpret our findings within the context of the prevailing nutrient (dissolved iron (dFe), nitrate, phosphate, and silicate) and light environments. We assess how the relative abundance of heme *b* varies in the ocean, where chl *a*: heme *b* ratios increase and how changes in the relative abundance of heme *b* proteins and light-harvesting complexes relate to nutrient distributions.

2. Methods

2.1. General

[7] Samples were obtained during three cruises in 2007 and 2008 (Figure 1 and Table 1). The IB cruise took place from 25 July to 19 August 2007. The cruise consisted of three repeat surveys of a 90 × 90 km grid in the North Atlantic subpolar gyre. The TNA cruise took place from 6 January to 3 February 2008. Samples were collected in the vicinity of the Canary and Cape Verde Islands, the subtropical North Atlantic Gyre and on a latitudinal transect along 12° N. The SS cruise took place from 1 January to 11 February 2008. Samples were collected in the vicinity of the South Orkney Islands, within the Antarctic Circumpolar Current (ACC) and in the bloom associated with South Georgia. Hydrographic data were collected with a Seabird 9/11 + conductivity-temperature-depth (CTD) on the IB and TNA cruises and with a Seabird SBE9 + CTD on the SS cruise.

2.2. Sample Collection

[8] Samples for heme *b*, chl *a*, POC, PON, and major nutrients were collected from depths < 250 m using a stainless steel CTD rosette equipped with 20 L Niskin (General Oceanics) bottles. Samples for dFe were collected using a trace metal clean titanium CTD rosette equipped with 12 L trace metal clean Teflon-coated OTE bottles or using a trace metal clean fish towed at approximately 5 m depth while the ship was steaming at 10 knots [*Nielsdottir et al*., 2012, 2009].

2.3. Particulate Heme *b*

[9] Between 1 and 4 L of seawater was filtered over 0.7 μm glass fiber filters (MF300, Fisher) and frozen (< −80°C) for analysis in the laboratory. An operationally defined fraction of the total intracellular heme *b* pool [*Honey et al*., 2013] was extracted into 1 mL of 0.02 M NH_4OH containing the zwitterionic detergent EMPIGEN (2.5% v/v, Sigma). Extracts were centrifuged, filtered (0.2 μm, Minisart, Sartorius), and determined spectrophotometrically after separation from other pigments by high-performance liquid chromatography [*Gledhill*, 2007; *Honey et al*., 2013]. Separations were performed using a polystyrene divinyl benzene stationary phase (PLRP-S column, 50 × 2.1 mm, 5 μm, Varian Inc.). High-performance liquid chromatography was carried out using binary gradient high-pressure pumps (Shimadzu, LC-10ADVPμ) and a diode array spectrophotometer equipped with a microcell (Shimadzu, SPD-M10AVP). The 100 μL of sample was injected onto the column using an autosampler (Shimadzu, SIL-10ADVP). The system was computer operated (LCsolution software) via a controller (Shimadzu, SCL-10AVP). Mobile phases consisted of (A) 20:20:40:0.1% (v:v:v:v) isopropanol (IPA): acetonitrile (ACN):water:nonafluoropentanoic acid (NFPA), and (B) 1:1:0.1 (v:v:v) IPA:ACN:NFPA. A standard gradient of 60% A to 100% B over 15 min, followed by 5 min isocratic elution with 100% B was used. The flow rate was 200 μL min^{-1}. Elution of heme *b* (retention time 5.5 min) was monitored by absorbance at 400 nm after applying a background absorbance correction using 450 nm in order to remove baseline fluctuations caused by EMPIGEN. Chromatograms and UV-visible light spectrometer spectra were routinely examined for the presence of other potential interfering pigments, which can be distinguished by shifts in the maximum absorption wavelength and the presence of secondary absorbance maxima. Heme *b* was quantified by comparison with standard solutions of iron (III) protoporphyrin IX chloride (Frontier Scientific). The detection limit for the

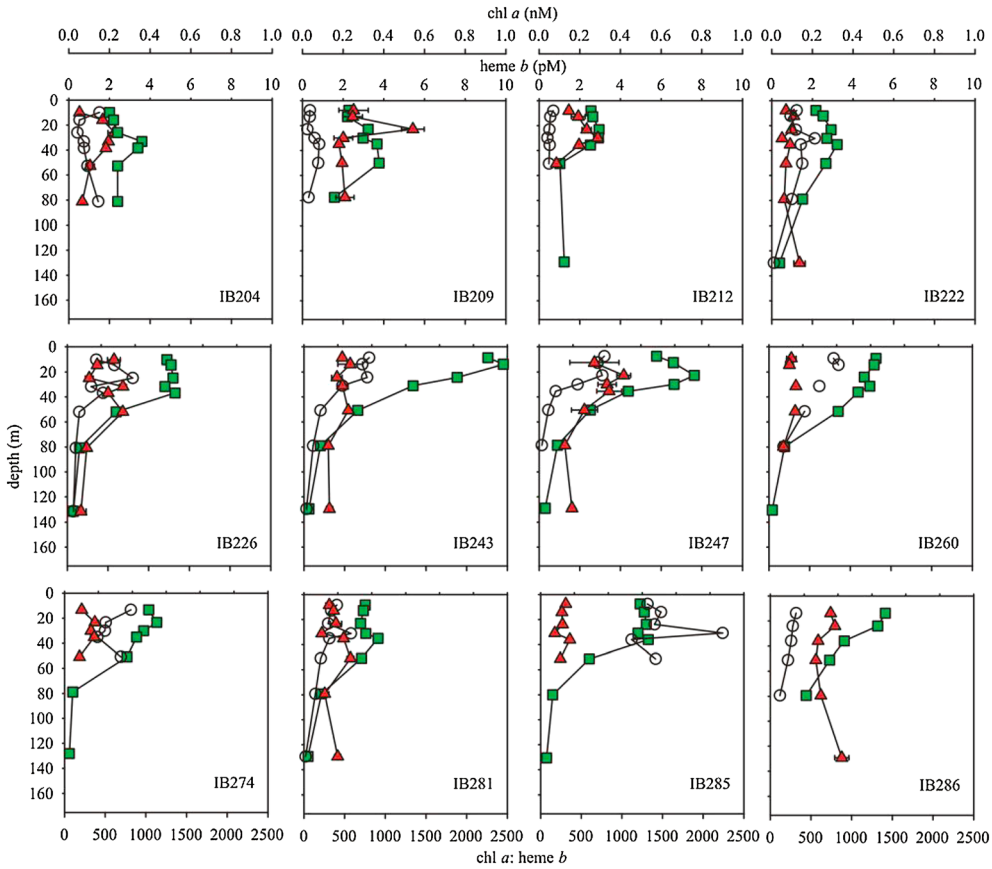

Figure 2. Vertical profiles for heme *b* (red triangles), chl *a* (green squares), and chl *a*:heme *b* (open circles) determined at stations in the Iceland Basin. Error bars for heme *b* represent the concentration range determined for each sample ($n = 2$).

technique was 1.6 nM. Extraction efficiency of heme *b* from human hemoglobin, horse skeletal myoglobin and human cytochrome b_5 (Sigma) proteins using ammoniacal EMPIGEN were assessed as described previously [*Honey et al*., 2013]. The extracted concentration of cytochrome b_5 was compared to the concentration determined from the difference spectrum for the reduced versus oxidized protein.

2.4. Chl *a*, F_v/F_m POC/PON, and Nutrients

[10] Water samples (100–200 mL) for chl *a* analysis were filtered over glass fiber filters (MF300, Fisher). Chlorophyll *a* was extracted into 10 mL of 90% (v/v) acetone over a 20–24 h period in the dark (4 °C). Chlorophyll *a* was determined by fluorometry (Turner Design TD-700) and calibrated using a pure chl *a* standard (spinach, Sigma). The maximum quantum yield (F_v/F_m) is reported here for dawn stations in the IB (IB222, IB226, IB260, and IB285) and SS. F_v/F_m was determined via chlorophyll fluorescence measurements obtained using fast repetition rate fluorometry (FRRF, Chelsea Scientific Instruments) and Fluorescence Induction and Relaxation (FIRe, Satlantic) [*Bibby et al*., 2008; *Kolber et al*., 1998]. Particulate organic carbon and PON were determined on the IB cruise following filtration of 1–2 L seawater onto precombusted glass fiber (0.7 μm; Whatman) filters [*Poulton et al*., 2006]. On the TNA cruise, POC and PON were determined at selected stations by mass spectrometry after filtration of up to 4 L seawater [*Moore et al*., 2006]. Macronutrients (nitrate + nitrite, hereafter termed nitrate, phosphate, and orthosilicic acid) were determined on board using an autoanalyzer and standard colorimetric techniques [*Sanders and Jickells*, 2000; *Whitehouse*, 1997] or in the TNA, with a nanomolar nutrient system following the method of *Patey et al*. [2008].

2.5. Dissolved Iron

[11] Dissolved iron was analyzed after gentle pressure filtration (0.2 μm) by an automated flow injection chemiluminescence method as previously described [*Nielsdottir et al*., 2012, 2009; *Obata et al*., 1993].

3. Results and Discussion

3.1. Heme *b* Extraction

[12] We have previously shown that ammoniacal detergent extraction of heme *b* is operational defined [*Honey et al*., 2013]. Comparison with total cellular iron indicated recoveries of 18 ± 14% of iron as heme *b*, consistent with the theoretical percentage of heme *b* in the photosystem proteins [*Gledhill*, 2007]. However, recoveries of heme *b* from catalase and horse radish peroxidase indicated that heme *b* extraction was below 40% for these hemoproteins. In this study, in order to better define ammoniacal detergent heme *b* extractions, we determined extraction efficiencies for three further readily available hemoproteins, hemoglobin, myoglobin, and mitochondrial cytochrome b_5. The results showed recoveries > 75–80% for extraction of heme *b* from

Table 2. Integrated Mixed-Layer Depth (MLD) Values for Heme *b* (nmol m^{-2}), Chlorophyll *a* (μmol m^{-2}), POC (mmol m^{-2}), and PON (mmol m^{-2}) Concentrations Calculated for Stations Sampled in the Iceland Basin, Tropical North Atlantic, and Scotia Sea

Station	Latitude (°N)	Longitude (°W)	Julian Day	MLD	Integrated Heme *b* (nmol m^{-2})	Integrated Chl *a* (μmol m^{-2})	Integrated POC (mmol m^{-2})	Integrated PON (mmol m^{-2})
				Iceland Basin				
IB204	59.99	19.86	210.04	43	65.3	9.96	356	58.7
IB209	59.69	20.41	211.13	31	102	7.2	365	55.3
IB212	59.71	18.75	212.09	33	67.4	8.1	288	39.7
IB222	58.86	19.88	214.10	31	26.7	7.1	209	27.3
IB226	58.84	21.01	216.97	35	38.5	15.7	368	50.6
IB243	59.86	20.46	221.55	31	39.8	26.9		
IB247	59.99	20.46	221.98	31	61.7	17.8	280	49.8
IB260	59.19	19.10	224.13	33	9.3	6.6	300	40.4
IB274	59.22	19.90	226.14	19	4.8	7.0	48	16.5
IB281	59.68	18.72	228.51	35	23.5	8.6	186	28.1
IB285	59.67	18.72	230.18	45	30.0	37.7	488	64.3
IB286	59.29	19.79	231.57	29	51.6	14.7	239	36.4
				Tropical Northeast Atlantic				
TNA389	25.59	24.10	8.83	104	270	26.1		
TNA390	25.95	25.59	9.23	126	106	21.0		
TNA397	22.83	27.19	12.63	107	209	22.2		
TNA398	20.91	26.12	13.29	97	194	25.2	243	24.6
TNA399	20.37	25.82	13.65	99	187	33.5		
TNA400	18.96	25.03	14.30	77	261	19.2		
TNA401	18.48	24.80	14.63	85	307	30.2		
TNA402	17.60	24.29	15.29	70	274	23.5	187	28.8
TNA402A	17.66	24.3	15.60	70	321	24.5		
TNA403	15.55	25.38	16.30	41	142	12.4		
TNA404	15.04	25.49	16.63	51	219	27.1		
TNA405	13.03	25.82	17.28	47	113	10.9		
TNA407	12.67	27.11	18.27	42	89.6	10.5		
TNA408	12.63	27.78	18.63	48	462	13.2		
TNA409	12.60	29.99	19.29	50	150	18.1	139	21.1
TNA410	12.59	30.60	19.64	64	196	23.5		
TNA411	12.55	32.67	20.30	51	150	13.0	159	27.4
TNA412	12.54	33.30	20.66	61	216	21.6		
TNA413	12.51	35.78	21.30	55	171	12.7	109	18.2
TNA414	12.54	35.31	21.65	67	121	18.2		
TNA415	12.61	33.24	22.30	48	111	13.8		
TNA416	12.59	32.61	22.66	70	69	16.1		
TNA417	12.51	30.61	23.41	71	187	16.1		
TNA418	16.12	30.63	24.50	62	89	12.4		
TNA419	16.16	30.63	25.28	56	84	9.5	121	21.2
TNA420	16.19	30.65	25.66	53	69	8.4		
TNA422	16.22	30.66	26.28	48	46	8.2	127	19.5
TNA423	16.20	30.62	26.63	48	37	7.5		
TNA425	16.23	30.65	27.28	43	87	8.5	95	14.3
TNA426	16.21	30.64	27.63	53	60	9.1		
TNA428	17.00	26.50	28.93	65	199	22.7		
TNA429	21.94	27.08	30.23	114	315	26.6	233	30.4
TNA430	22.82	27.19	30.64	129	208	20.0		
TNA431	25.07	28.47	31.31	126	127	28.5	205	27.7
TNA432	26.16	26.41	32.39	139	324	29.4	201	27.4
TNA433	26.59	23.72	33.27	147	345	35.3	269	38.6
TNA434	26.71	23.01	33.64	150	199	38.2		
TNA435	27.14	20.44	34.25	129	354	24.68		
				Scotia Sea				
SSC2	−60.20	44.41	8.38	21	90	20.6		
SSC4	−58.02	42.98	19.29	42	315	26.2		
SSP24	−55.90	41.72	23.5	63	109	47.1		
SSP28	−54.59	41.00	29.4	67	159	83.7		
SSP3	−52.85	40.10	32.3	63	867	211		
SSR3	−52.63	39.11	35.3	41	138	212		

hemoproteins such as globins and cytochromes using ammoniacal detergent (Table 1). This is likely related to the heme *b* ligand environment, spin state, and the degree to which the heme group is likely to be exposed to the solvent (Table 1) and is consistent with the known lability of heme *b* in hemoproteins, previously reported heme *b* to cellular iron ratios and the observed relationship between heme *b* and the photosystem II protein PsbA [*Frausto da Silva and Williams*,

Table 3. Results of Pearson Product Moment Correlation for Heme *b*, Chl *a*, Particulate Organic Carbon (POC), and Particulate Organic Nitrogen (PON) in the Iceland Basin, Tropical Northeast Atlantic, and Scotia Sea[a]

	Chl *a*	POC	PON
	Iceland Basin		
Heme *b* r (*n*)	0.19 (84)	0.41 (77)	0.45 (77)
p	0.08	<0.01	<0.01
Chl *a r* (*n*)		0.66 (79)	0.6 (79)
p		<0.01	<0.01
POC *r* (*n*)			0.99 (79)
p			<0.01
	Tropical Northeast Atlantic		
Heme *b r* (*n*)	0.41 (269)	0.23 (60)	
p	<0.01	0.07	0.43(60)
			<0.01
Chl *a r* (*n*)		0.19 (60)	0.38 (60)
p		0.15	<0.01
POC *r* (*n*)			0.60 (64)
p			<0.01
	Scotia Sea		
Heme *b r* (*n*)	0.27 (34)		
p	0.13		

[a]No POC/PON data were collected for the Scotia Sea.

2001; *Honey et al*., 2013; *Weber et al*., 2011]. Therefore, heme *b* concentrations determined using our method are likely to be strongly influenced by the abundance of *b*-type cytochromes, which in phytoplankton include cytb_6f, cytochrome b_5, and cytochrome bc_1. In addition, it is possible that the intracellular location of heme will also play a role in extraction efficiency. Thus, although not fully quantitative, variation in our heme *b* concentrations will reflect variation in the cytochrome content and thus changes in the potential for electron transport within phytoplankton populations.

3.2. Surface Heme *b*, Chl *a*, POC, and PON in the Iceland Basin

[13] Particulate heme *b* concentrations in the IB ranged from < 0.4 to 5.3 pM, averaging 1.18 ± 0.8 pM (± 1 standard deviation; $n = 86$). Depth profiles showed some enhanced concentrations in surface waters, but trends were not as strong as for chl *a* (Figure 2). Integrated mixed-layer depth values for chl *a*, heme *b*, POC, and PON calculated for the IB are given in Table 2. Heme *b* concentrations in the IB were found to correlate weakly with POC and PON; however, no significant correlation was observed with chl *a* (Table 3). Comparison of mixed-layer depth-integrated heme *b* concentrations with phytoplankton carbon (phyC) [*Poulton et al*., 2010] indicated that heme *b*:phyC ratios were between 0.07 and 0.78 μmol mol^{-1}, considerably lower than ratios observed in phytoplankton grown under nutrient replete conditions in the laboratory (average 3.7 ± 0.9 μmol mol^{-1}) and lower than those reported previously for the Celtic Sea [*Honey et al*., 2013]. The low concentration of heme *b* in this region was also reflected in the heme *b*:POC and heme *b*:PON ratios (Table 3). The low concentrations of heme *b* with respect to carbon indicate that the abundance of *b*-type cytochromes was also low and is compatible with the low F_v/F_m values (Table 4) observed in the mixed layer in this region at the time of sampling. Phytoplankton have been found to decrease their heme *b*:POC ratios in response to nutrient limitation [*Honey et al*., 2013]. At station IB285, situated in the center of a cyclonic eddy, low heme *b*:POC ratios (0.06 ± 0.01 μmol mol^{-1}) were not reflected in decreases in chl *a*:POC (~ 80 μmol mol^{-1}), which were close to the average obtained for the IB (107 ± 24 μmol mol^{-1}). The decrease in heme *b*:POC thus led to an integrated mixed-layer chl *a*:heme *b* ratio of 1260 at this station. Integrated chl *a*:heme *b* ratios > 500 were also observed at stations IB260 and IB274, and again, coincided with low heme *b*:POC ratios (0.07 ± 0.01 and 0.09 ± 0.03 μmol mol^{-1}, respectively). Coccolithophores, dominated by *Emiliania huxleyi* made up between 10 and 25% of the phytoplankton carbon at the time of this study [*Poulton et al*., 2010]. Chl *a* to heme *b* ratios in *E. huxleyi* have been observed to increase under low-iron and/or -light conditions in the laboratory [*Honey et al*., 2013]. Average daily irradiances in the IB during the cruise ranged between 9 and 39 mol photosynthetically active radiation m^{-2} d^{-1} and were not thought to be limiting phytoplankton growth in the mixed layer [*Poulton et al*., 2010]. The concentrations of nitrate and phosphate at stations IB260, IB274, and within the cyclonic eddy were also not fully depleted (average mixed-layer depth concentrations at these stations: 3.6 ± 2.1 μM nitrate, 0.29 ± 0.1 μM phosphate, 0.5 ± 0.4 μM silicate). Mixed-layer depth dFe concentrations averaged 0.016 ± 0.01 nM at the cyclonic eddy station and 0.05 ± 0.01 nM at station IB260 (no dFe determined at station IB274), constituting the lowest dFe concentrations detected during the IB study. The high chl *a*:heme *b* ratios observed in the IB are therefore most likely a response of the phytoplankton population to the low dFe concentrations observed at stations IB260, IB274, and in the cyclonic eddy.

3.3. Surface Heme *b*, Chl *a*, POC, and PON in the Tropical North Atlantic

[14] Particulate heme *b* in the TNA averaged 2.24 ± 1.67 pM ($n = 275$) and were very similar to those observed in 2010 in this region [*Honey et al*., 2013]. Minimum concentrations were below the detection limit (< 0.4 pM), while the maximum concentration observed in this region was 19.4 pM. Depth profiles were similar to those of chl *a*, with enhanced concentrations in the photic zone (Figure 3). In the TNA, there was a weak correlation between heme *b* and PON, but no significant relationship between heme *b* and

Table 4. Comparison of Heme *b*:PhyC Ratio With F_v/F_m Observed in the Iceland Basin and Scotia Sea

	Heme *b*:PhyC (μmol mol^{-1})	F_v/F_m
	Iceland Basin[a]	
Station		
IB222	0.24	0.27 ± 0.02
IB226	0.33	0.27 ± 0.02
IB260	0.04	0.24 ± 0.01
IB285	0.09	0.29 ± 0.01
	Scotia Sea[b]	
Station		
SSC2	2.4	0.39
SSC4	4.1	0.25
SSP24	0.5	0.19
SSP28	0.5	0.28
SSP3	5.5	0.56
SSR3	0.4	0.39

[a]Integrated mixed-layer heme *b*:phyC ratios are compared with average mixed-layer F_v/F_m values.
[b]Values for heme *b*:phyC ratios and F_v/F_m for samples collected at 20 m.

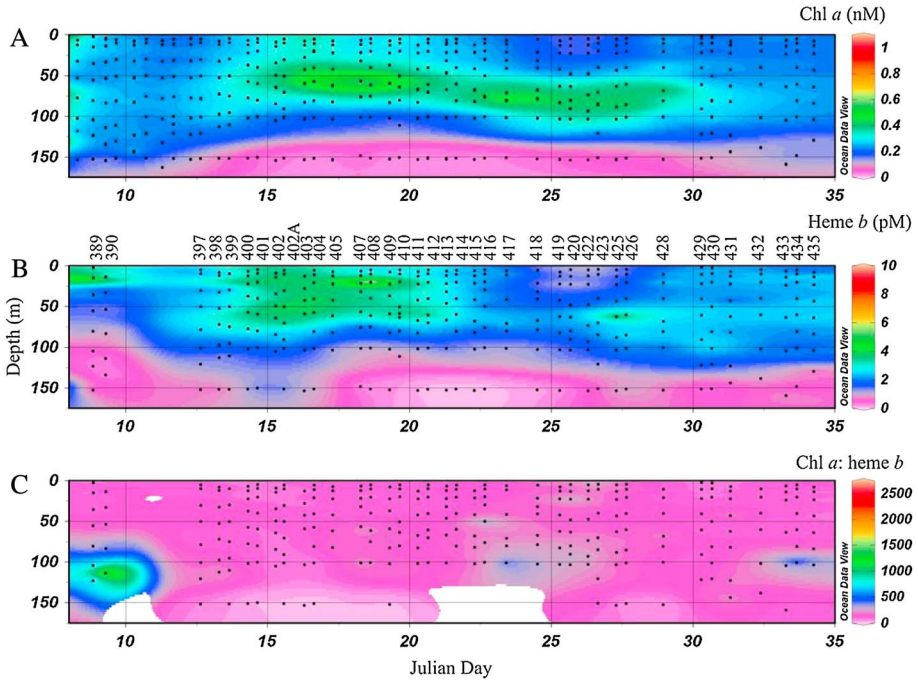

Figure 3. Contour plot for vertical sections of (a) chl *a* concentration (nM), (b) heme *b* concentration (pM), and (c) chl *a*:heme *b* determined in the tropical North Atlantic. Station numbers are indicated on Figure 3b.

POC (Table 3). Integrated mixed-layer depth values for chl *a*, heme *b*, POC, and PON calculated for the TNA are given in Table 2. Mixed-layer heme *b*:POC and heme *b*:PON ratios were higher (1.0 ± 0.5 and $7.6 \pm 2.9\ \mu\text{mol mol}^{-1}$, respectively) than values observed for the IB, although still lower than heme *b*:POC ratios observed for nutrient replete phytoplankton in the laboratory [*Honey et al*., 2013]. There was no overall change in heme *b*:POC with depth (data not shown), indicating that light was unlikely to be influencing the level of heme *b* in this region, despite the presence of a deep chlorophyll maximum at some stations in the TNA study area. Chl *a* to POC ratios were also higher (average $134 \pm 80\ \mu\text{mol mol}^{-1}$) in the TNA compared to the IB (Table 2). A significant correlation between heme *b* and chl *a* was observed in the TNA samples (Table 3) consistent with previously reported results [*Honey et al*., 2013]. Chl *a* to heme *b* ratios in the TNA were below 500, except for four isolated samples (Figure 3c). The frequency of samples at depth with high chl *a*:heme *b* ratios makes it difficult to identify a cause, although the heme *b* concentrations detected in these samples were likely to be subject to greater error as they were close to the detection limit of the heme *b* technique. Integrated mixed-layer depth chl *a*:heme *b* ratios averaged 124 ± 45, similar to ratios reported previously for the region [*Honey et al*., 2013] and considerably lower than those observed in the IB. Nitrate and phosphate concentrations were very low in surface waters in the TNA (3–50 nM nitrate, 2–90 nM phosphate) and are likely to limit growth in the region [*Moore et al*., 2009]. A correlation between these limiting nutrients and heme *b* has been reported for a transect across the (sub-) tropical North Atlantic Ocean [*Honey et al*., 2013]; however, in this study no significant correlation was observed, likely a result of the reduced spatial scale of the survey.

[15] On 14 days in the TNA, samples were collected both at dawn and midafternoon (Table 1). Although these samples were not collected from the same waters, afternoon (1500–1700 GMT) mixed-layer depth chl *a*:heme *b* ratios were higher than dawn (0700 GMT) ratios on 11 of the 14 days (Figure 4). These results indicate that diurnal variation in the production of chl *a* and heme *b* may be occurring, with heme *b* production lower during the day relative to chl *a* as a result of optimization of the chl *a*/heme *b* biosynthetic pathway [*Papenbrock et al*., 1999; *Tanaka and Tanaka*, 2007]. The lack of concurrent POC/PON data does not allow for examination of potential diurnal cycling of the overall abundance of heme *b* proteins, which has been reported in laboratory cultures [*Saito et al*., 2011].

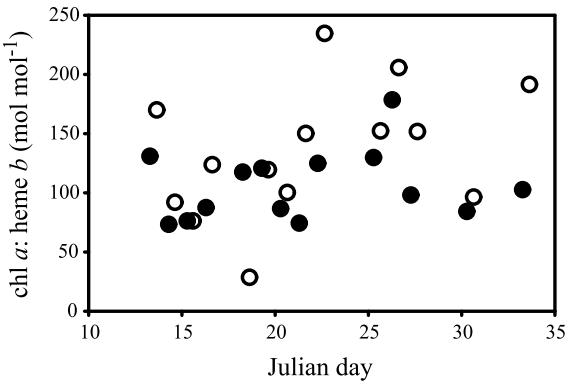

Figure 4. Integrated mixed-layer depth chl *a*:heme *b* ratios during the day in the tropical northeast Atlantic where stations were sampled at dawn (0700 GMT, dark circles) and midafternoon (1500–1700 GMT, open circles).

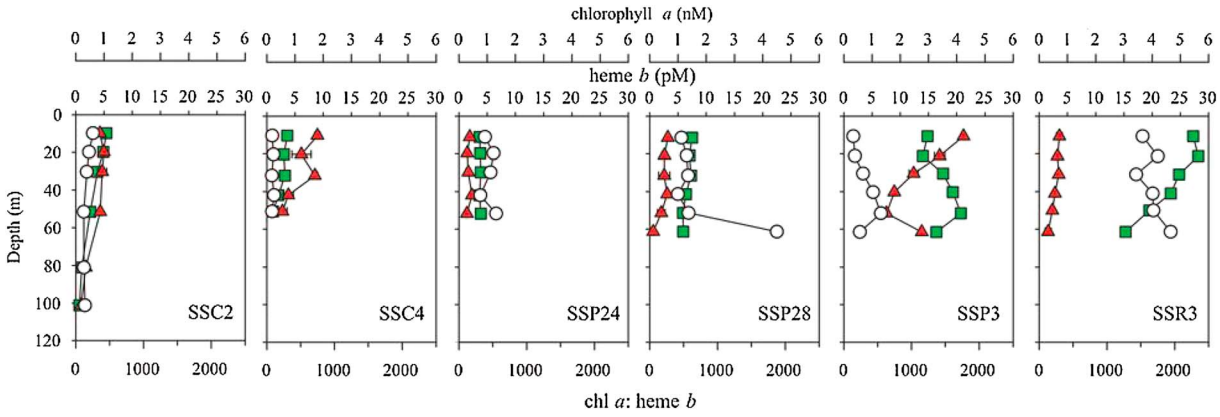

Figure 5. Vertical profiles for heme *b* concentrations (red triangles), *c*hl *a* concentrations (green squares), and chl *a*:heme *b* ratio (open circles) calculated for stations in the Scotia Sea. Error bars for heme *b* represent the concentration range determined for each sample ($n = 2$).

3.4. Surface Heme *b* and Chl *a* in the Scotia Sea

[16] Heme *b* concentrations in the SS varied from 0.6 to 21 pM with an average of 1.9 ± 1.7 pM and were thus higher than those determined in the IB (Figure 5). Particulate organic carbon and PON were not determined for the SS samples. Phytoplankton counts were undertaken at a depth of 20 m at each station [*Korb et al.*, 2010] and heme *b* concentrations were therefore compared to the calculated phytoplankton carbon biomass (phyC). However, it should be noted that these calculations do not include the biomass from nanoeukaryotes or picoeukaryotes and are thus likely to overestimate actual heme *b*:phyC ratios. Results of the comparison are reported in Table 4. Heme *b* to phyC ratios observed at SSC2, SSC4, and SSP3 were similar to heme *b*:C ratios observed in nutrient replete phytoplankton grown in the laboratory [*Honey et al.*, 2013]. Bioassay experiments carried out close to SSC2 and SSP3 indicated that phytoplankton were not iron limited [*Hinz et al.*, 2012]. The low heme *b*:phyC ratio observed at stations SSP24, SSP28, and SSR3 to the northwest of South Georgia and in the SS indicates that the phytoplankton community was growing under low-nutrient conditions at these stations. Iron bioassay experiments near station SSP24 indicated that the phytoplankton community was iron limited in this area [*Hinz et al.*, 2012]. The estimates of heme *b*:phyC determined for stations in the SS are broadly compatible with changes in F_v/F_m recorded in the region (Table 4). F_v/F_m was highest around station SSR3, where the highest heme *b*:phyC ratio was observed. Furthermore, south of South Georgia at stations SSP24 and SSP28, F_v/F_m was also observed to be lower (<0.3, Table 4), consistent with the depleted heme *b*:phyC ratios. However, at other stations (SSC2, SSC4, and SSP3) with similar F_v/F_m values, we observed a wide variability in heme *b*:phyC ratios. This could have been a result of underestimation of the heme *b*:phyC ratio due to omission of C from nanoeukaryotes and picoeukaryotes, likely to be especially important at SSC2 and SSC4, as these areas were dominated by small phytoplankton species [*Korb et al.*, 2011]. In addition, comparison between F_v/F_m and heme *b*:phyC in the region is also likely influenced by changes in the community composition [*Suggett et al.*, 2009] as the dominant taxonomic groups varied from cryptophytes at station SSC2, dinoflagellates at SSC4, and diatoms at SSP24, SSP28, SSP3, and SSR3 [*Korb et al.*, 2010, 2011]. It was notable that chl *a*:phyC ratios at stations SSP24, SSP28, and SSR3 were close to the average observed for all the stations (252, 265, and 590 μmol mol^{-1}, respectively), showing that while heme *b* was depleted relative to biomass at these stations, chl *a* was not. Integrated mixed-layer depth values for chl *a* and heme *b* calculated for the SS are given in Table 2. Chlorophyll *a* to heme *b* ratios ranged between 80 and 1940, with a mean value of 533 (Figure 5). As with the IB, no significant correlation between heme *b* and chl *a* was observed (Table 3). Integrated chl *a*:heme *b* ratios were below 500 north of the South Orkney Islands and increased going north across the SS to a value of 528 just south of South Georgia. West of South Georgia mixed-layer chl *a*:heme *b* ratios decreased to 240. This region is strongly influenced by iron inputs from the South Georgia Ridge and the station sampled was close to an area reported to be iron replete at the time of sampling (Figure 6) [*Hinz et al.*, 2012]. Northwest of

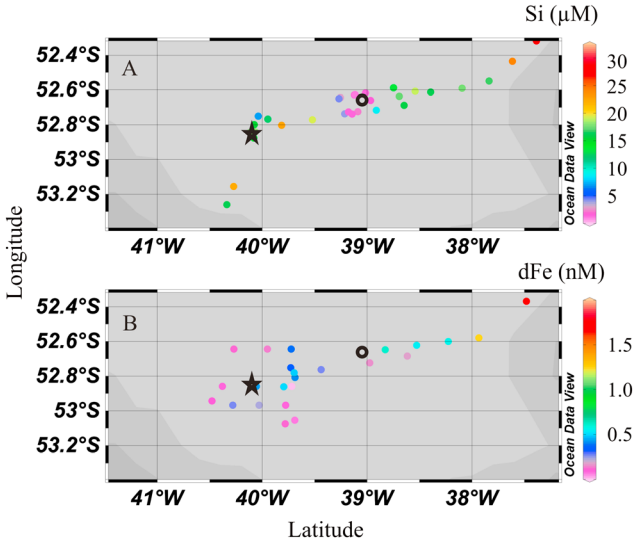

Figure 6. Surface distribution of (a) dissolved Si and (b) dissolved iron northwest of South Georgia in relation to stations SSP3 (star) and SSR3 (circle).

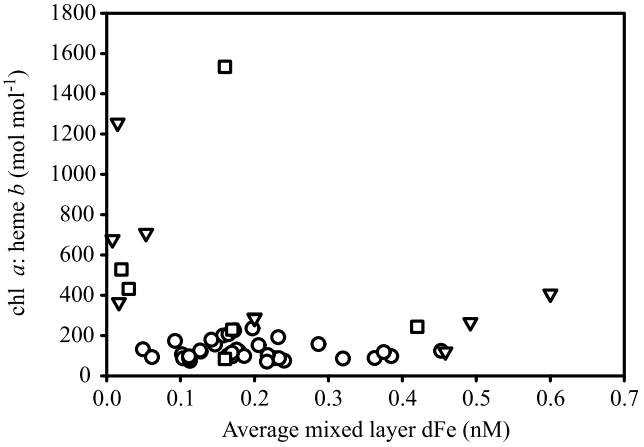

Figure 7. Integrated chl *a*:heme *b* ratios plotted against average mixed-layer dFe concentrations. Iceland Basin—inverted triangles, tropical northeast Atlantic—circles, and Scotia Sea —squares. For the Scotia Sea, the closest dFe concentrations collected with underway sampling system were used.

South Georgia, however, we observed high chl *a*:heme *b* ratios (> 1400), combined with low heme *b*:phyC ratios. This station (SSR3) was characterized by high chl *a* (~ 5 μg L^{-1}), complete drawdown of Si (< 0.15 μM) and relatively depleted N concentrations (~ 14 μM). The phytoplankton community at both stations was dominated by diatoms [*Korb et al*., 2010, 2011]; however, F_v/F_m was lower at SSR3 than at SSP3 (Table 4). Dissolved iron concentrations were not recorded at the station itself; however, comparison of dFe and nutrient data showed that the closest underway dFe samples (situated 15 and 27 km to the southwest of the station; upstream in the ACC) had dFe concentrations of 0.16 ± 0.01 nM and 0.61 ± 0.1 nM, respectively (Figure 6). The phytoplankton community at SSR3 was dominated by centric diatoms over 10 μm in size [*Korb et al*., 2010] which are thought to have relatively high iron requirements [*Ho et al*., 2003; *Sunda and Huntsman*, 1995]. Therefore, it is possible that the phytoplankton at this station have exhausted the nutrient supply to the extent that they have reduced their hemoprotein content.

3.5. Implications of Changes in Intracellular Heme *b* for Marine Phytoplankton

[17] This study reports the first investigation into the distribution of heme *b* in iron-limited marine environments. In the Atlantic and Southern Oceans, we have observed variations in heme *b* concentrations ranging from < 0.2 to 21 pM. Heme *b* distributions reflected changes in phytoplankton biomass, with higher heme *b* concentrations observed in regions of higher biomass. However, the concentration of heme *b* relative to the organic carbon and nitrogen and to chl *a* varied considerably between the three areas surveyed. Our study indicates that variations of heme *b*:POC ratio reflect changes in the abundance of heme *b* proteins such as cytb_6f, PSII, and eukaryotic nitrate reductase in particulate material while variations in chl *a*:heme *b* ratio will reflect changes in the relative capacity for light harvesting versus electron transport. Laboratory studies have shown that heme *b*:POC decreases when marine phytoplankton are grown under low-nutrient conditions. Species specific increases in chl *a*:heme *b* ratios were also observed in phytoplankton grown under low-nutrient and low-light conditions [*Honey et al*., 2013]. In the IB and SS to the south of South Georgia, chl *a*:heme *b* ratios over 500 were observed at stations with low dFe concentrations (Figure 7). The high chl *a*:heme *b* ratios resulted mainly from a relative reduction in heme *b* abundance. Although dFe concentrations in the SS to the northwest of South Georgia were not as low as those in the IB and south of South Georgia, we suggest that the low Si concentrations coupled to the higher iron demand of the dominant large centric diatoms led to the enhanced chl *a*:heme *b* ratios. In this study, we have highlighted increases in the chl *a*:heme *b* ratio to values > 500, which are in excess of chl *a*:heme *b* ratios we have observed in the laboratory [*Honey et al*., 2013]. Observed increases in chl *a*:heme *b* to values > 500 were associated with particular stations (e.g., IB285 and SSR3) which were not observed to have major shifts in species composition when compared to other nearby stations [*Korb et al*., 2010; *Poulton et al*., 2010]. This suggests that the change in chl *a*:heme *b* ratio in the IB and SS resulted from a physiological response, rather than a shift in species composition. However, the absence of high chl *a*:heme *b* ratios in the TNA may not be influenced solely by the higher dFe and heme *b*:POC ratios in this region when compared to the SS and IB but is also likely to reflect large-scale changes in phytoplankton community composition as biomass in this region is dominated by prokaryotes which utilize different light-harvesting strategies [*Ting et al*., 2002].

[18] The chl *a*:heme *b* ratios reported here are likely consistent with the adaptation of the photosystem to the prevailing light and nutrient conditions, within the context of large-scale changes in phytoplankton community dynamics. Our results indicate that the abundance of heme *b* and thus cytochromes with respect to biomass and other photosystem complexes are likely to change. Although we cannot be certain which cytochromes are most affected, a reduction in cytb_6f would be particularly crucial as it connects the two photosynthetic reaction center complexes and is involved in linear and cyclic electron transfer [*Baniulis et al*., 2008; *Iwai et al*., 2010]. Cytochrome b_6f proteins and genes have been shown to be downregulated in some phytoplankton when iron stressed [*Strzepek and Harrison*, 2004; *Thompson et al*., 2011]. Cytochrome b_6f potentially plays a contributory role in regulating electron transport through the process of "photosynthetic control" [*Eberhard et al*., 2008; *Peltier et al*., 2010]. Furthermore, in green algae, cytb_6f regulates state transitions and the switching of light-harvesting complexes from PSII to PSI thus changing the amount of linear versus cyclic electron transport [*Lemeille and Rochaix*, 2010]. Gaining insight into cytb_6f abundance in the ocean and its relationship to other photosystem complexes will shed light on fundamental electron transport processes occurring in the ocean, and how these impact on productivity.

[19] Our investigation into heme *b* distributions has shown that heme *b*:POC and chl *a*:heme *b* ratios vary with biomass and nutrient distributions. We have identified stations in the SS and IB where phytoplankton have high chl *a*:heme *b* as a result of low-nutrient concentrations. Our study shows that low dFe is the most likely cause of high chl *a*:heme *b* ratios in the IB, while a combination of low dFe and Si contributes to high chl *a*:heme *b* ratios in the SS. Furthermore, our results indicate that there are changes in the abundance of heme *b* proteins such as cytochromes in the phytoplankton

communities in the IB and the SS as a result of low-nutrient concentrations. Changes in the abundance of cytochromes will affect electron transport and thus potentially influence the efficiency of photosynthesis and productivity of phytoplankton communities. Determination of particulate heme *b* in the ocean and comparison with POC, biomass, or chl *a* thus contributes to our understanding of the dynamics of phytoplankton blooms and adaptation of phytoplankton communities to prevailing growth conditions in the ocean.

[20] **Acknowledgments.** The authors gratefully acknowledge all the comments made by the anonymous reviewers of this work. This work was supported by a NERC Advanced Fellowship grant awarded to MG (NE/E013546/1). The authors would like to thank the officers, crew, and scientists of the R.R.S. *Discovery* and R.R.S. *James Clark Ross* during cruises D321, D326, and JR177. We would like to thank M. Patey for the nutrient data from the tropical North Atlantic; S. Henson and A. Poulton for the satellite images; A. Poulton for phytoplankton counts and taxanomic data; C.M. Moore and M. Lucas for particulate organic matter data; and C.M. Moore and T.S. Bibby for supplying the F_v/F_m data.

References

Allen, A. E., J. LaRoche, U. Maheswari, M. Lommer, N. Schauer, P. J. Lopez, G. Finazzi, A. R. Fernie, and C. Bowler (2008), Whole-cell response of the pennate diatom Phaeodactylum tricornutum to iron starvation, *Proc. Natl. Acad. Sci. U. S. A.*, *105*, 10,438–10,443, doi:10.1073/pnas.0711370105.

Bailey, S., A. Melis, K. R. M. Mackey, P. Cardol, G. Finazzi, G. van Dijken, G. M. Berg, K. Arrigo, J. Shrager, and A. Grossman (2008), Alternative photosynthetic electron flow to oxygen in marine Synechococcus, *Biochim. Biophys. Acta*, *1777*, 269–276, doi:10.1016/j.bbabio.2008.01.002.

Banci, L., I. Bertini, B. R. Branchini, P. Hajieva, G. A. Spyroulias, and P. Turano (2001), Dimethyl propionate ester heme-containing cytochrome $b_{(5)}$: Structure and stability, *J. Biol. Inorg. Chem.*, *6*, 490–503, doi:10.1007/s007750100217.

Baniulis, D., E. Yamashita, H. Zhang, S. S. Hasan, and W. A. Cramer (2008), Structure-function of the cytochrome $b_{(6)}f$ complex, *Photochem. Photobiol.*, *84*, 1349–1358, doi:10.1111/j.1751-1097.2008.00444.x.

Berglund, G. I., G. H. Carlsson, A. T. Smith, H. Szoke, A. Henriksen, and J. Hajdu (2002), The catalytic pathway of horseradish peroxidase at high resolution, *Nature*, *417*, 463–468, doi:10.1038/417463a.

Bibby, T. S., M. Y. Gorbunov, K. W. Wyman, and P. G. Falkowski (2008), Photosynthetic community responses to upwelling in mesoscale eddies in the subtropical North Atlantic and Pacific Oceans, *Deep Sea Res., Part II*, *55*, 1310–1320, doi:10.1016/j.dsr2.2008.01.014.

Cardol, P., et al. (2008), An original adaptation of photosynthesis in the marine green alga Ostreococcus, *Proc. Natl. Acad. Sci. U. S. A.*, *105*, 7881–7886, doi:10.1072/pnas.0802762105.

Chapman, S. K., S. Daff, and A. W. Munro (1997), Heme: The most versatile redox centre in biology?, in *Metal Sites in Proteins and Models*, edited by H. A. O. Hill et al., pp. 39–70, Springer, Berlin, Heidelberg.

Chiapello, I., G. Bergametti, L. Gomes, B. Chatenet, F. Dulac, J. Pimenta, and E. S. Suares (1995), An additional low layer transport of Sahelian and Saharan dust over the north-eastern tropical Atlantic, *Geophys. Res. Lett.*, *22*, 3191–3194, doi:10.1029/95GL03313.

Doty, M. S., and M. Oguri (1956), The island mass effect, *J. Cons.*, *22*, 33–37, doi:10.1093/icesjms/22.1.33.

Eberhard, S., G. Finazzi, and F. A. Wollman (2008), The dynamics of photosynthesis, *Annu. Rev. Genet.*, *42*, 463–515, doi:10.1146/annurev.genet.42.110807.091452.

Erdner, D. L., and D. M. Anderson (1999), Ferredoxin and flavodoxin as biochemical indicators of iron limitation during open-ocean iron enrichment, *Limnol. Oceanogr.*, *44*, 1609–1615, doi:10.4319/lo.1999.44.7.1609.

Espinas, N. A., K. Kobayashi, S. Takahashi, N. Mochizuki, and T. Masuda (2012), Evaluation of unbound free heme in plant cells by differential acetone extraction, *Plant Cell Physiol.*, *53*, 1344–1354, doi:10.1093/pcp/pcs067.

Foroughi, L. M., Y.-N. Kang, and A. J. Matzger (2011), Polymer-induced heteronucleation for protein single crystal growth: Structural elucidation of Bovine liver catalase and Concanavalin A forms, *Cryst. Growth Des.*, *11*, 1294–1298, doi:10.1021/cg101518f.

Frausto da Silva, J., and R. Williams (2001), *The Biological Chemistry of the Elements*, pp. 575, Oxford Univ. Press, New York.

Gledhill, M. (2007), The determination of heme b in marine phyto- and bacterioplankton, *Mar. Chem.*, *103*, 393–403, doi:10.1016/j.marchem.2006.10.008.

Hersleth, H.-P., T. Uchida, A. K. Rohr, T. Teschner, V. Schünemann, T. Kitagawa, A. X. Trautwein, C. H. Görbitz, and K. K. Andersson (2007), Crystallographic and spectroscopic studies of peroxide-derived myoglobin compound II and occurrence of protonated FeIV-O*, *J. Biol. Chem.*, *282*, 23,372–23,386, doi:10.1074/jbc.M701948200.

Hill, P. G., M. V. Zubkov, and D. A. Purdie (2010), Differential responses of Prochlorococcus and SAR11-dominated bacterioplankton groups to atmospheric dust inputs in the tropical northeast Atlantic Ocean, *FEMS Microbiol. Lett.*, *306*, 82–89, doi:10.1111/j.1574-6968.2010.01940.x.

Hinz, D. J., M. C. Nielsdottir, R. E. Korb, M. J. Whitehouse, A. J. Poulton, C. M. Moore, E. P. Achterberg, and T. S. Bibby (2012), Responses of microplankton community structure to iron addition in the Scotia Sea, *Deep Sea Res., Part II*, *59-60*, 36–46, doi:10.1016/j.dsr2.2011.08.006.

Ho, T. Y., A. Quigg, Z. V. Finkel, A. J. Milligan, K. Wyman, P. G. Falkowski, and F. M. M. Morel (2003), The elemental composition of some marine phytoplankton, *J. Phycol.*, *39*, 1145–1159, doi:10.1111/j.0022-3646.2003.03-090.x.

Honey, D. J., M. Gledhill, T. S. Bibby, F. E. Legiret, N. J. Pratt, A. E. Hickman, T. Lawson, and E. P. Achterberg (2013), Heme b in marine phytoplankton and particulate material from the North Atlantic Ocean, *Mar. Ecol. Prog. Ser.*, *483*, 1–17, doi:10.3354/meps10367.

Iwai, M., K. Takizawa, R. Tokutsu, A. Okamuro, Y. Takahashi, and J. Minagawa (2010), Isolation of the elusive supercomplex that drives cyclic electron flow in photosynthesis, *Nature*, *464*, 1210–U1134, doi:10.1038/nature08885.

Jickells, T. D., et al. (2005), Global iron connections between desert dust, ocean biogeochemistry, and climate, *Science*, *308*, 67–71, doi:10.1126/science.1105959.

Kolber, Z. S., O. Prasil, and P. G. Falkowski (1998), Measurements of variable chlorophyll fluorescence using fast repetition rate techniques: Defining methodology and experimental protocols, *Biochim. Biophys. Acta.*, *1367*, 88–106, doi:10.1016/S0005-2728(98)00135-2.

Korb, R. E., M. J. Whitehouse, S. E. Thorpe, and M. Gordon (2005), Primary production across the Scotia Sea in relation to the physico-chemical environment, *J. Mar. Syst.*, *57*, 231–249, doi:10.1016/j.jmarsys.2005.04.009.

Korb, R. E., M. J. Whitehouse, M. Gordon, P. Ward, and A. J. Poulton (2010), Summer microplankton community structure across the Scotia Sea: Implications for biological carbon export, *Biogeosciences*, *7*, 343–356, doi:10.5194/bg-7-343-2010.

Korb, R. E., M. J. Whitehouse, P. Ward, M. Gordon, H. J. Venables, and A. J. Poulton (2011), Regional and seasonal differences in microplankton biomass, productivity, and structure across the Scotia Sea: Implications for the export of biogenic carbon, *Deep Sea Res., Part II*, *59–60*, 67–77, doi:10.1016/j.dsr2.2011.06.006.

Leblanc, K., et al. (2009), Distribution of calcifying and silicifying phytoplankton in relation to environmental and biogeochemical parameters during the late stages of the 2005 north east Atlantic spring bloom, *Biogeosciences*, *6*, 2155–2179, doi:10.5194/bg-6-2155-2009.

Lemeille, S., and J. D. Rochaix (2010), State transitions at the crossroad of thylakoid signalling pathways, *Photosynth. Res.*, *106*, 33–46, doi:10.1007/s11120-010-9538-8.

Lommer, M., et al. (2012), Genome and low-iron response of an oceanic diatom adapted to chronic iron limitation, *Genome Biol.*, *13*(7), R66, doi:10.1186/gb-2012-13-7-r66.

Mckay, R. M. L., J. LaRoche, A. F. Yakunin, D. G. Durnford, and R. J. Geider (1999), Accumulation of ferredoxin and flavodoxin in a marine diatom in response to Fe, *J. Phycol.*, *35*, 510–519, doi:10.1046/j.1529-8817.1999.3530510.x.

Moore, C. M., M. M. Mills, A. Milne, R. Langlois, E. P. Achterberg, K. Lochte, R. J. Geider, and J. LaRoche (2006), Iron limits primary productivity during spring bloom development in the central North Atlantic, *Global Change Biol.*, *12*, 626–634, doi:10.1111/j.1365-2486.2006.01122.x.

Moore, C. M., et al. (2009), Large-scale distribution of Atlantic nitrogen fixation controlled by iron availability, *Nat. Geosci.*, *2*, 867–871, doi:10.1038/NGEO667.

Mulitza, S., et al. (2010), Increase in African dust flux at the onset of commercial agriculture in the Sahel region, *Nature*, *466*, 226–228, doi:10.1038/nature09213.

Nielsdottir, M. C., C. M. Moore, R. Sanders, D. J. Hinz, and E. P. Achterberg (2009), Iron limitation of the postbloom phytoplankton communities in the Iceland Basin, *Global Biogeochem. Cycles*, *23*, GB3001, doi:10.1029/2008GB003410.

Nielsdottir, M., T. S. Bibby, C. M. Moore, D. J. Hinz, R. Sanders, M. J. Whitehouse, R. E. Korb, and E. P. Achterberg (2012), Seasonal dynamics of iron availability in the Scotia Sea, *Mar. Chem.*, *130-131*, 62–72, doi:10.1016/j.marchem.2011.12.004.

Obata, H., H. Karatani, and E. Nakayama (1993), Automated determination of iron in sea water by chelating resin concentration and chemiluminescence detection, *Anal. Chem.*, *65*, 1524–1528, doi:10.1021/ac00059a007.

Pankowski, A., and A. McMinn (2009), Development of immunoassays for the iron-regulated proteins ferrodoxin and flavodoxin in polar microalgae, *J. Phycol.*, *45*, 771–783, doi:10.1111/j.1529-8817.2009.00687.x.

Paoli, M., R. Liddington, J. Tame, A. Wilkinson, and G. Dodson (1996), Crystal structure of T state haemoglobin with oxygen bound at all four haems, *J. Mol. Biol.*, *256*, 775–792, doi:10.1006/jmbi.1996.0124.

Papenbrock, J., H. P. Mock, E. Kruse, and B. Grimm (1999), Expression studies in tetrapyrrole biosynthesis: Inverse maxima of magnesium chelatase and ferrochelatase activity during cyclic photoperiods, *Planta*, *208*, 264–273, doi:10.1007/s004250050558.

Patey, M. D., M. J. A. Rijkenberg, P. J. Statham, M. C. Stinchcombe, E. P. Achterberg, and M. Mowlem (2008), Determination of nitrate and phosphate in seawater at nanomolar concentrations, *Trends Anal. Chem.*, *27*, 169–182, doi:10.1016/j.trac.2007.12.006.

Peers, G., and N. M. Price (2006), Copper-containing plastocyanin used for electron transport by an oceanic diatom, *Nature*, *441*, 341–344, doi:10.1038/nature04630.

Peltier, G., D. Tolleter, E. Billon, and L. Cournac (2010), Auxiliary electron transport pathways in chloroplasts of microalgae, *Photosynth. Res.*, *106*, 19–31, doi:10.1007/s11120-010-9575-3.

Poulton, A. J., P. M. Holligan, A. Hickman, Y. N. Kim, T. R. Adey, M. C. Stinchcombe, C. Holeton, S. Root, and E. M. S. Woodward (2006), Phytoplankton carbon fixation, chlorophyll-biomass and diagnostic pigments in the Atlantic Ocean, *Deep Sea Res., Part II*, *53*, 1593–1610, doi:10.1016/j.dsr2.2006.05.007.

Poulton, A. J., A. Charalampopoulou, J. R. Young, G. A. Tarran, M. I. Lucas, and G. D. Quartly (2010), Coccolithophore dynamics in non-bloom conditions during late summer in the central Iceland Basin (July–August 2007), *Limnol. Oceanogr.*, *55*, 1601–1613, doi:10.4319/lo.2010.55.4.1601.

Rijkenberg, M. J. A., R. J. Langlois, M. M. Mills, M. D. Patey, P. G. Hill, M. C. Nielsdottir, T. J. Compton, J. LaRoche, and E. P. Achterberg (2011), Environmental forcing of nitrogen fixation in the eastern tropical and sub-tropical North Atlantic Ocean, *PloS ONE*, *6*(13), e28989, doi:10.1371/journal.pone.0028989.

Rijkenberg, M. J. A., S. Steigenberger, C. F. Powell, H. van Haren, M. D. Patey, A. R. Baker, and E. P. Achterberg (2012), Fluxes and distribution of dissolved iron the eastern (sub-) tropical North Atlantic Ocean, *Global Biogeochem. Cycles*, *26*, GB3004, doi:10.1029/2011GB004264.

Saito, M. A., E. M. Bertrand, S. Dutkiewicz, V. V. Bulygin, D. M. Moran, F. M. Monteiro, M. J. Follows, F. W. Valois, and J. B. Waterbury (2011), Iron conservation by reduction of metalloenxyme inventories in the marine diazotroph Crocosphaera watsonii, *Proc. Natl. Acad. Sci. U. S. A.*, *108*, 2184–2189, doi:10.1073/pnas.1006943108.

Sanders, R., and T. Jickells (2000), Total organic nutrients in Drake Passage, *Deep Sea Res., Part I*, *47*, 997–1014, doi:10.1016/S0967-0637(99)00079-5.

Shekhawat, G. S., and K. Verma (2010), Haem oxygenase (HO): An overlooked enzyme of plant metabolism and defence, *J. Exp. Bot.*, *61*, 2255–2270, doi:10.1093/jxb/erq074.

Stramma, L., P. Brandt, J. Schafstall, F. Schott, J. Fischer, and A. Kortzinger (2008), Oxygen minimum zone in the North Atlantic south and east of the Cape Verde Islands, *J. Geophys. Res.*, *113*, C04014, doi:10.1029/2007JC004369.

Strzepek, R. F., and P. J. Harrison (2004), Photosynthetic architecture differs in coastal and oceanic diatoms, *Nature*, *431*, 689–692, doi:10.1038/nature02954.

Stuut, J. B., M. Zabel, V. Ratmeyer, P. Helmke, E. Schefuss, G. Lavik, and R. Schneider (2005), Provenance of present-day aeolian dust collected off NW Africa, *J. Geophys. Res.*, *110*, D04202, doi:10.1029/2004JD005161.

Suggett, D. J., C. M. Moore, A. E. Hickman, and R. J. Geider (2009), Interpretation of fast repetition rate (FRR) fluorescence: Signatures of phytoplankton community structure versus physiological state, *Mar. Ecol. Prog. Ser.*, *376*, 1–19, doi:10.3354/meps07830.

Sunda, W. G., and S. A. Huntsman (1995), Iron uptake and growth limitation in oceanic and coastal phytoplankton, *Mar. Chem.*, *50*, 189–206, doi:10.1016/0304-4203(95)00035-P.

Tanaka, R., and A. Tanaka (2007), Tetrapyrrole biosynthesis in higher plants, *Annu. Rev. Plant Biol.*, *58*, 321–346, doi:10.1146/annurev.arplant.57.032905.105448.

Thompson, A. W., K. Huang, M. A. Saito, and S. W. Chisholm (2011), Transcriptome response of high- and low-light-adapted Prochlorococcus strains to changing iron availability, *The ISME J.*, *5*, 1580–1594, doi:10.1038/ismej.2011.49.

Ting, C. S., G. Rocap, J. King, and S. W. Chisholm (2002), Cyanobacterial photosynthesis in the oceans: The origins and significance of divergent light-harvesting strategies, *Trends Microbiol.*, *10*, 134–142, doi:10.1016/s0966-842x(02)02319-3.

Weber, M., A. Prodohl, C. Dreher, C. Becker, J. Underhaug, A. S. P. Svane, A. Malmendal, N. C. Nielsen, D. Otzen, and D. Schneider (2011), SDS-facilitated in vitro formation of a transmembrane b-type cytochrome is mediated by changes in local pH, *J. Mol. Biol.*, *407*, 594–606, doi:10.1016/j.jmb.2011.02.005.

Whitehouse, M. J. (1997), *Automated Seawater Nutrient Chemistry*, British Antarctic Survey, Cambridge, U. K.

Wolfe-Simon, F., V. Starovoytov, J. R. Reinfelder, O. Schofield, and P. G. Falkowski (2006), Localization and role of manganese superoxide dismutase in a marine diatom, *Plant Physiol.*, *142*, 1701–1709, doi:10.1104/pp.106.088963.